This is intended as a review paper only and it summarizes work which has been submitted for publication in the *IEEE Transactions on MTT*.

PROGRESS IN INTEGRATED-CIRCUIT HORN ANTENNAS FOR RECEIVER APPLICATIONS

PART 1: Antenna Design

George V. Eleftheriades, Walid Y. Ali-Ahmad, and Gabriel M. Rebeiz

NASA/Center for Space Terahertz Technology
Electrical Engineering and Computer Science Department
University of Michigan
Ann Arbor, MI 48109-2122

ABSTRACT

The purpose of this work is to present a systematic method for the design of multimode quasi-integrated horn antennas. The design methodology is based on the Gaussian beam approach and the structures are optimized for achieving maximum fundamental Gaussian coupling efficiency. For this purpose, a hybrid technique is employed in which the integrated part of the antennas is treated using full-wave analysis, whereas the machined part is treated using an approximate method. This results in a simple and efficient design process. The developed design procedure has been applied for the design of a 20dB, a 23dB and a 25dB quasi-integrated horn antennas, all with a Gaussian coupling efficieny exceeding 97%. The designed antennas have been tested and characterized using both full-wave analysis and 90GHz/370GHz measurements.

I. QUASI-INTEGRATED HORN ANTENNA DESIGN : INTRODUCTION

The integrated-circuit horn antenna was introduced in [1] and analyzed using a full-wave analysis technique in [2]. It consists of a dipole (or monopole) feed evaporated on a thin dielectric membrane which is suspended in a pyramidal cavity etched in silicon or GaAs. Recently, this antenna has been used in several millimeter and submillimeter-wave applications including a double-polarized antenna design at 93GHz [4], a 256 element imaging array at 802GHz [5], and a monopulse tracking system at 94GHz [6]. However, the wide flare-angle of the integrated-circuit horn antenna, which is dictated by the anisotropic etching involved in its fabrication (70° in silicon), limits its useful aperture size to 1.6λ and its gain to 13dB. To this end the quasi-integrated horn antenna was introduced [3], which consists of a machined small flare-angle pyramidal section attached to the integrated portion (fig.1). The resulting structure is a simple multimode pyramidal horn with circularly symmetric patterns, high gain, and low cross-polarization, which is particularly attractive for submillimeter quasi-optical receiver applications. The minimum machined dimension involved in its fabrication is around 1.5λ which enables its fabrication to frequencies up to 2THz. The purpose of this paper is to describe a systematic approach towards the design of these horn antennas, and to provide a full range of practical quasi-integrated horn antenna designs along with their detailed radiation characteristics. Since a very desirable property of antennas intended for use in quasi-optical systems is the high Gaussian content of their radiated fields [7], the developed design methodology is based on the optimization of the quasi-integrated horns for achieving maximum fundamental Gaussian coupling efficiency. The Gaussian coupling efficiency is particularly important in quasi-optical receiver applications because it directly influences the total system performance with a pronounced effect on the receiver noise temperature [8].

II. MULTIMODE APERTURE ANALYSIS FOR MAXIMUM FUNDAMENTAL COUPLING EFFICIENCY

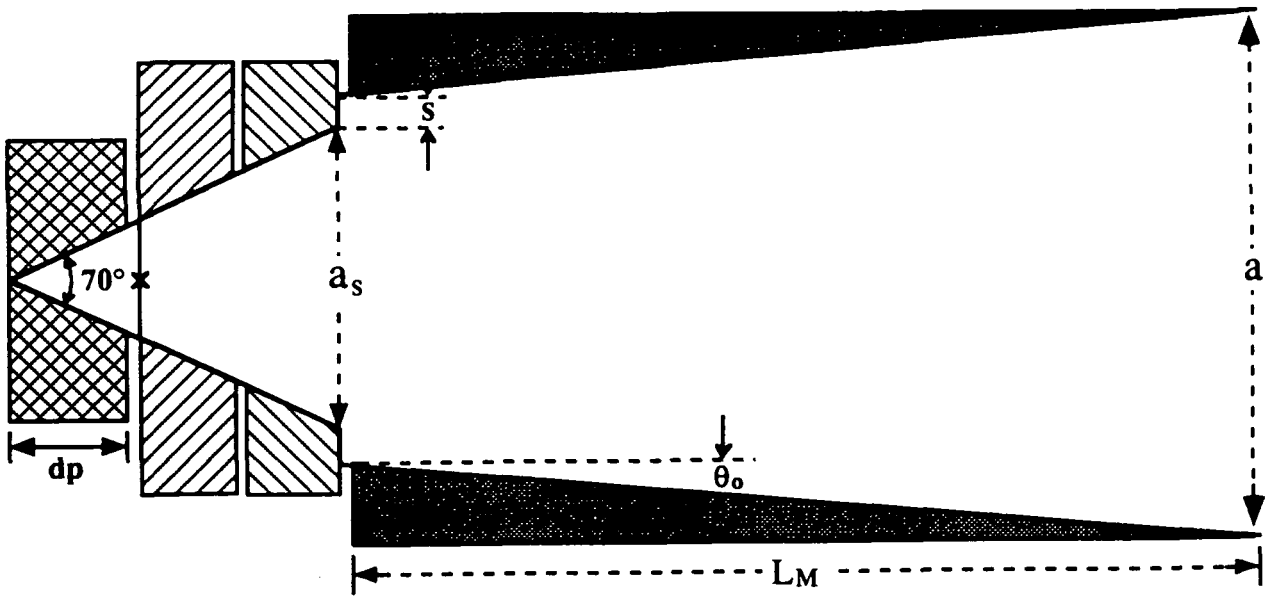

Fig.1 The general configuration of the quasi-integrated multimode horn antenna.

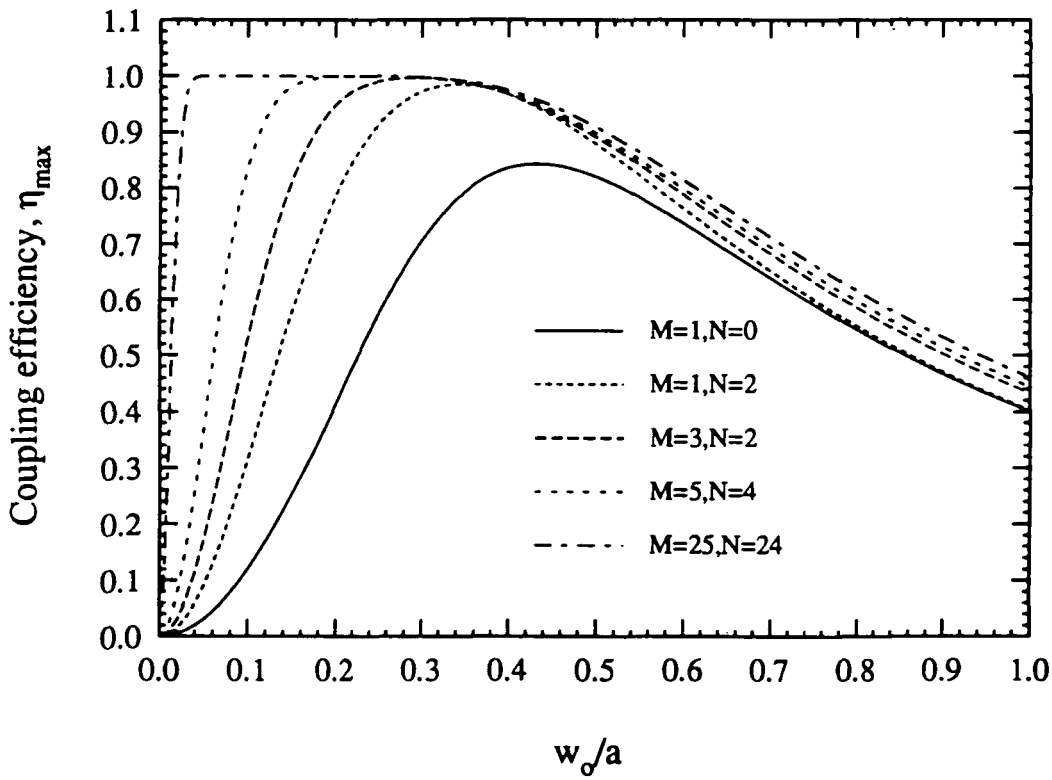

Fig.2 The maximum Gaussian coupling efficiency as a function of the w_o/a ratio for various aperture modes available for beamshaping (up to $TE_{M,N}/TM_{M,N}$, $m = 1, 3 \ldots M$, $n = 0, 2 \ldots N$) .

Consider a square aperture of side a in a ground-plane which is radiating in the half-space $z > 0$. The transverse electric field of the aperture at $z = 0$ can be expanded in terms of the eigenfunctions of a square waveguide of the same side a :

$$\bar{E}_{t,ap}(x,y) = \sum_{m,n}^{M,N} \{A_{mn}\bar{e}^{TE}_{mn}(x,y) + C_{mn}\bar{e}^{TM}_{mn}(x,y)\} \quad . \tag{1}$$

In (1) it is assumed that only modes with indices ($m = 1,3,5 \ldots M$ and $n = 0,2,4,6 \ldots N$) are present as is the case of a pyramidal horn which is either fed by a centered Hertzian dipole or by a waveguide which supports only the dominant TE_{10} mode [2]. We now proceed to determine the modal coefficients A_{mn}, B_{mn} so that the coupling between the aperture field and a fundamental beam is maximized. If the copolarized and cross-polarized components of the aperture field are defined to be the $\bar{E}_{x,ap}$ and the $\bar{E}_{y,ap}$ components respectively, then the transverse electric field can be rewritten in the form :

$$E_{y,ap}(x,y) = \sum_{m,n}^{M,N} d^{co}_{mn}\Psi^{co}_{mn}(x,y) \quad , E_{x,ap}(x,y) = \sum_{m,n}^{M,N} d^{xp}_{mn}\Psi^{xp}_{mn}(x,y) \tag{2}$$

where the orthonormalized copolarized and cross-polarized hybrid modes Ψ^{co}_{mn}, Ψ^{xp}_{mn} are:

$$\Psi^{co}_{mn}(x,y) = \frac{\sqrt{2\epsilon_n}}{a}(-1)^{\frac{m+n-1}{2}} \cos(\frac{m\pi x}{a}) \cos(\frac{n\pi y}{a}) \quad , |x| \leq a/2, |y| \leq a/2 \tag{3}$$

$$\Psi^{xp}_{mn}(x,y) = \frac{\sqrt{2\epsilon_n}}{a}(-1)^{\frac{m+n+1}{2}} \sin(\frac{m\pi x}{a}) \sin(\frac{n\pi y}{a}) \quad , |x| \leq a/2, |y| \leq a/2 \tag{4}$$

In (3) and (4) the origin of the Cartesian coordinates is located at the geometrical center of the aperture and $\epsilon_n = 2 - \delta_{n0}$ is the Neumann number. The corresponding copolarized and cross-polarized modal coefficients of (3-4) are related to the modal coefficients of (1) through:

$$d^{co}_{mn} = \frac{nC_{mn} - mA_{mn}}{\sqrt{m^2+n^2}} \quad , d^{xp}_{mn} = \frac{nA_{mn} + mC_{mn}}{\sqrt{m^2+n^2}}. \tag{5}$$

Now the coupling efficiency $\eta(w_o)$ of the aperture to a fundamental Gaussian beam of waist radius w_o, which has its waist on the aperture is given by [11] :

$$\eta(w_o) = \left| \sum_{m,n}^{M,N} d^{co}_{mn} I_{mn}(w_o) \right|^2 / \left(\frac{w_o^2\pi}{2} \sum_{m,n}^{M,N} (|d^{cp}_{mn}|^2 + |d^{xp}_{mn}|^2)\right) \tag{6}$$

$$\text{where,} \quad I_{mn}(w_o) = \iint_{apert.} \Psi^{co}_{mn}(x,y) exp(-(x^2+y^2)/w_o^2)\, dx\, dy. \tag{7}$$

We wish at this point to determine the modal coefficients d^{co}_{mn} and d^{xp}_{mn} so that the coupling efficiency $\eta(w_o)$ is maximized. For this purpose, the application of Schwarz's inequality to (6) immediately implies that the maximum coupling efficiency $\eta_{max}(w_o)$ occurs in the absence of cross-polarization and is obtained from :

$$\eta_{max}(w_o) = \frac{2}{w_o^2 \pi} \sum_{m,n}^{M,N} |I_{mn}(w_o)|^2 \tag{8}$$

with the corresponding co-polarization modal coefficients determined by :

$$d^{co}_{mn} \;/\; I_{mn}(w_o) = \text{constant}. \tag{9}$$

The condition for vanishing cross-polarization is (see 5) : $\quad nA_{mn} = -mC_{mn}$. (10)

Therefore, for maximum fundamental Gaussian coupling efficiency the aperture modes should add in phase and their relative magnitudes should satisfy conditions (9) and (10). The maximum coupling efficiency $\eta_{max}(w_o)$ of equation (9) still depends on the waist radius w_o and it is shown in figure 2 as a function of the ratio w_o/a for various indices (M,N). In table 1 we show the relative magnitudes between the modes at the optimum $w_{o,opt}/a$ ratio, for some practically encountered aperture sets of modes.

Available modes (M,N)	(1,0)	(1,2)	(1,2)+TE_{30}	(3,2)
$w_{o,opt}/a$	0.43	0.34	0.32	0.29
cpl. efficiency : η_{max}	84%	98.5%	99.2%	99.7%
d^{co}_{12}/d_{10}	-	0.51	0.56	0.64
d^{co}_{30}/d_{10}	-	-	0.11	0.17
d^{co}_{32}/d_{10}	-	-	-	-0.11

Table 1: Optimum parameters for maximum fundamental Gaussian coupling efficiency for certain practically encountered aperture modes available for beamshaping.

III. APPROXIMATE ANALYSIS OF THE MACHINED SECTION AND DESCRIPTION OF THE DESIGN PROCESS

Consider the gradually-flared pyramidal machined section of axial length L_M and of half flare-angle θ_o (see fig. 1) which is assumed excited at its throat by M × N locally propagating modes. Since the machined section is gradually flared and the incident modes propagating, reflections at the throat are considered negligible and the corresponding transverse electric field is given by :

$$\bar{E}_{t,thr}(x,y) = \sum_{m,n}^{M,N} \{A_{mn}^{th} \bar{e}_{mn}^{th,TE}(x,y) + C_{mn}^{th} \bar{e}_{mn}^{th,TM}(x,y)\} \quad . \tag{11}$$

To a first order approximation we can assume that each mode preserves its carried power upon propagating from the throat to the aperture. Also, each mode acquires a phase shift computed by :

$$\Phi_{mn} = \int_0^{L_M} \beta_{mn}(z)\, dz \tag{12}$$

where $\beta_{mn}(z)$ is the local propagation constant of the mn^{th}-mode. The above phase shift has been used extensively for the design of multimode horns [9-10] and it can be rigorously justified through a coupled-mode analysis of gradually flared tapers [13]. The aperture field is assumed to be modulated by a quadratic phase factor $Q_{L_T}(x,y)$ of curvature $L_T = a/(2\tan\theta_o)$ with L_T being the total virtual length of the taper. Under the above assumptions and neglecting reflections , the aperture field is simply given by :

$$\bar{E}_{t,ap}(x,y) = Q_{L_T}(x,y) \sum_{m,n}^{M,N} \{\acute{A}_{mn}^{ap} \bar{e}_{mn}^{ap,TE}(x,y) + \acute{C}_{mn}^{ap} \bar{e}_{mn}^{ap,TM}(x,y)\} \tag{13}$$

with the quadratically modulated aperture modal coefficients related to the throat modal coefficients through :

$$\acute{A}_{mn}^{ap} = A_{mn}^{th} \sqrt{Y_{mn}^{th,TE}/Y_o} \exp(-j\Phi_{mn}) \quad , \acute{C}_{mn}^{ap} = C_{mn}^{th} \sqrt{Y_{mn}^{th,TM}/Y_o} \exp(-j\Phi_{mn}) \tag{14}$$

where Y_{mn}^{th} is the throat admittance for the mn^{th} mode and Y_o is the free-space intrinsic admittance which has been assigned to the aperture modes. Based on the above simplified analysis for

the machined section and on a full-wave analysis of the integrated portion a three-stage design process has been established and is summarized below :

1. The integrated 70° flare-angle section of the antenna structure of figure 1 (including the step discontinuity) is selected and analyzed independently of the machined section. For this purpose, the dipole-fed integrated portion is assumed to be terminated by an infinite square waveguide of side $(a_s + 2s)$ and is analyzed using the full-wave analysis technique of [2] to obtain the throat modal coefficients A^{th}_{mn}, C^{th}_{mn}. The junction cross-section a_s and the step size s (see fig. 1) are selected so that the *magnitudes* of the radiating aperture modal coefficients, as predicted by equations 5 and 14, satisfy the optimal conditions (9) and (10) as closely as possible.

2. The infinite waveguide is now replaced by the gradually flared machined section and the assumption is made that the modal coefficients at the throat of the machined section retain their computed values of stage 1. This is a good approximation since the actual excited modal coefficients are determined by the difference between the integrated portion flare-angle and the machined section flare-angle and this difference is always dominated by the large 70° flare-angle of the integrated portion [10]. The length L_M and the flare-angle θ_o of the machined section are then selected iteratively (using 12) so that the modal coefficients $\dot{d}^{co}_{mn}$ appear in phase on the radiating aperture. The shortest possible length is chosen in order to achieve the maximum bandwidth.

3. Finally, the length and the flare-angle of the machined section are "fine-tuned" using the full-wave analysis of [2] for the entire quasi-integrated horn antenna and again for achieving maximum Gaussian coupling efficiency.

In table 2 we quantify several practical geometries of integrated portions which have resulted from the first stage of the design process.

IV. NUMERICAL AND EXPERIMENTAL RESULTS FOR SPECIFIC QUASI-INTEGRATED HORN ANTENNA DESIGNS.

The algorithm of section III has been employed for the design of a 20dB, a 23dB and a 25dB quasi-integrated horn antenna, all with a fundamental Gaussian coupling efficiency exceeding 97% and with a full-null beam efficiency around 99%. Although, in the design process the analysis of the machined section is performed using the approximate method of section III, the computation of the radiation characteristics of the finally designed horns is carried out using the full-wave analysis technique of [2]. Furthermore, using this full-wave analysis along with 6GHz scale-model measurements it was verified that the input impedance of the feeding strip-dipole in the integrated portion of the horn is not affected by the attachment of the machined section [3]. This is due to the fact that the input impedance of the feeding strip is mainly determined by its local geometrical environment which remains unaffected by the attachment of the machined section. The input impedance for the integrated-circuit horn antennas has already been analyzed theoretically and characterized experimentally in [2] where it was shown that by adjusting the dipole position inside the horn, the input impedance can be matched to either Schottky or SIS diodes. Therefore, the results of [2] are directly applicable to the case of the quasi-integrated horn antennas as well.

A. 20dB quasi-integrated horn antenna.

The geometrical parameters for the 20dB realization are calculated to be ($a_s = 1.35\lambda, s = 0.0, L_M = 7\lambda, \theta_o = 9°, dp = 0.39\lambda$) and the numerically computed patterns from the third stage of the design process along with the corresponding 90GHz measurements have been reported in [3]. In fig. 3 the principal patterns are compared to the patterns obtained by analyzing the machined section using the approximate method of section III. As shown, the approximate model agrees well with both the full-wave analysis and the measurements thus verifying the approximations used in the design process. The main radiation characteristics of this horn at

the design frequency and at the edges of the ±5% bandwidth are summarized in table 3. The indicated 10-dB beamwidth fluctuation corresponds to the variation of the beamwidth in an azimuthal far-field cut. The Gaussian-beam rolloff was calculated at the edges of the ±5% bandwidth using the Gaussian-beam parameters which were calculated at the design frequency f_o. The calculated phase center was found to be located at a distance of 1.5λ from the horn aperture for the E-plane and at 1.4λ for the H-plane.

B. 23dB quasi-integrated horn antenna.

The optimized design parameters for a 23dB quasi-integrated horn are found to be ($a_s = 1.52\lambda, s = 0.17\lambda, L_M = 13\lambda, \theta_o = 8.5^o$, $dp = 0.39\lambda$) and the computed principal patterns from both the full-wave analysis of the entire antenna and from the approximate model of section III are compared in figure 4 to corresponding 370GHz measurements. In figure 5 we include also the computed from the full-wave analysis and the measured patterns for the 45^o-plane. The radiation characteristics of this horn are being summarized in table 4. For the 23dB horn the phase center was calculated to be at 3.7λ inside the horn for the E-plane and at 3.5λ for the H-plane.

C. 25dB Quasi-integrated horn antenna.

In order to evaluate the efficiency of the design process and to provide a full range of practical designs, a 25dB quasi-integrated horn has also been designed and the computed geometrical parameters are found to be: ($a_s = 1.52\lambda, s = 0.0\lambda, L_M = 19.5\lambda, \theta_o = 10^o$, $dp = 0.39\lambda$). The radiation patterns, as calculated from the full-wave analysis and shown in figure 6 still exhibit excellent circular symmetry, low cross-polarization and suppressed sidelobes. The location of the phase center for this horn was computed to be at a distance of 13λ from the aperture for the E-plane and at 11λ for the H-plane. The rest of the main radiation characteristics of this horn antenna are being tabulated in table 5.

	Optimum	$a_s = 1.35\lambda$ $s = 0.0$	$a_s = 1.52\lambda$ $s = 0.0$	$a_s = 1.35\lambda$ $s = 0.17\lambda$	$a_s = 1.57\lambda$ $s = 0.0$
$\lvert\acute{d}_{12}^{co,ap}\rvert/\lvert\acute{d}_{10}^{ap}\rvert$	0.56*	0.52	0.50	0.55	0.51
$\lvert\acute{d}_{30}^{ap}\rvert/\lvert\acute{d}_{10}^{ap}\rvert$	0.114	-	0.11	0.117	0.146
$arg(\acute{C}_{12}^{ap}/\acute{A}_{12}^{ap})$	180°	200°	183°	182°	179°
$\lvert\acute{C}_{12}^{ap}\rvert/\lvert\acute{A}_{12}^{ap}\rvert$	2	4.5	4.4	5.1	4.3

Table 2: Comparison between the optimum aperture modal coefficients and the modal coefficients launched at the aperture by four practical integrated portion sections. The exciting dipole is positioned at a distance of 0.39λ from the apex of the horn. * The optimum ratio $\lvert\acute{d}_{12}^{co,ap}\rvert/\lvert\acute{d}_{10}^{ap}\rvert$ is 0.51 for the $a_s = 1.35\lambda$ geometry which only triggers the $TE_{10}, TE_{12}/TM_{12}$ modes.

	$0.95f_o$	f_o	$1.05f_o$
Gain	19.4dB	20dB	20.6dB
Aperture efficiency	60.6%	62.8%	65.4%
10dB Beamwidth	$37° \pm 1°$	$34° \pm 1.2°$	$32° \pm 1.8°$
Sidelobe-level (E-plane)	−23dB	−27dB	−26.3dB
Cross-pol.(45°)	−22.5dB	−22.7dB	−23dB
Beam-efficiency (to -10dB)	85%	86%	86.5%
Gaussian Coupling	96.4%	97.3%	96.9%
Gaussian Coupling rolloff	95.5%	97.3%	96.5%

Table 3: The main radiation characteristics of the 20dB quasi-integrated horn antenna (see text).

	$0.965f_o$	f_o	$1.035f_o$
Gain	22.2dB	22.8dB	23.6dB
Aperture efficiency	48.5%	52%	58.4%
10dB Beamwidth	$27.6 \pm 0.2°$	$25° \pm 1.1°$	$22.5° \pm 1.3°$
Sidelobe-level (E-plane)	−28dB	−33dB	−29.8dB
Cross-pol.(45°)	−20.5dB	−21dB	−22dB
Beam-efficiency (to -10dB)	86.6%	86%	86.6%
Gaussian Coupling	97.2%	97.3%	96.8%
Gaussian Coupling rolloff	96.3%	97.3%	96.0%

Table 4: The main radiation characteristics of the 23dB quasi-integrated horn antenna (see text).

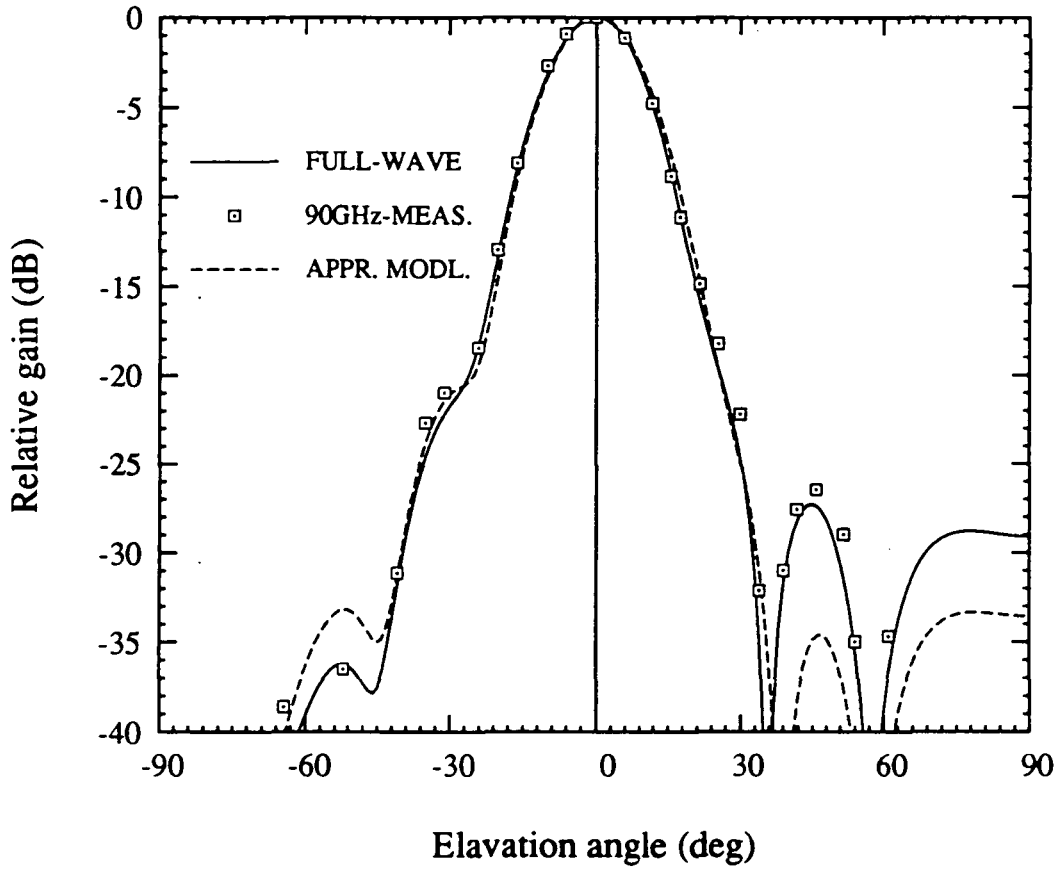

Fig.3 The E (right) and H-plane (left) patterns of the 20-dB quasi-integrated horn. The 90GHz measured patterns are compared to the full-wave analysis and the approximate analysis patterns. Detailed patterns including cross-polarization are shown in [3].

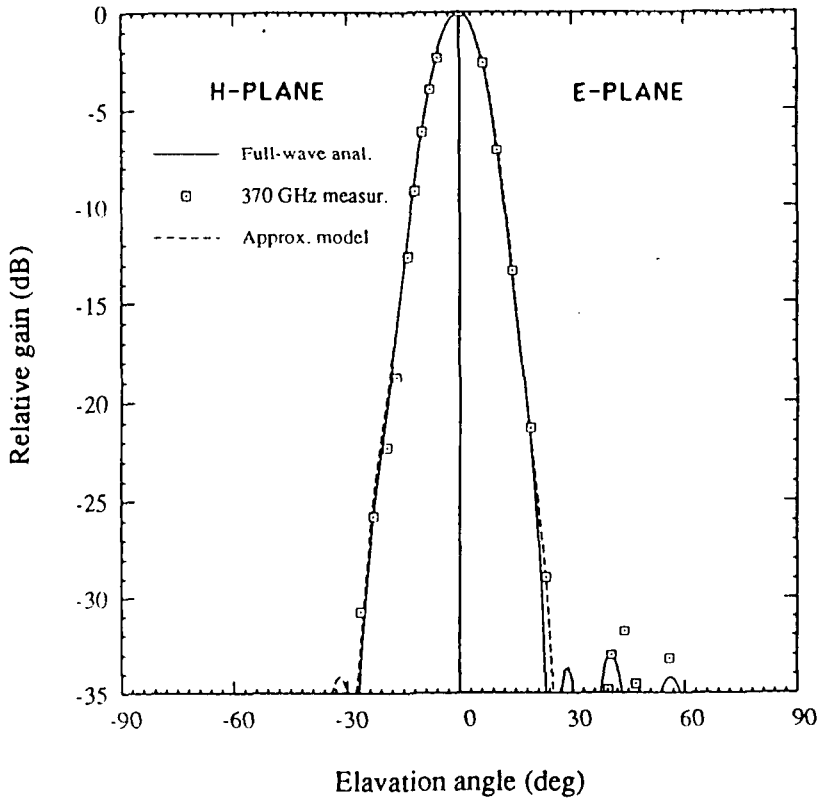

Fig.4 The E (right) and H-plane (left) patterns of the 23-dB quasi-integrated horn. The 370GHz measured patterns are compared to the full-wave analysis and the approximate analysis patterns.

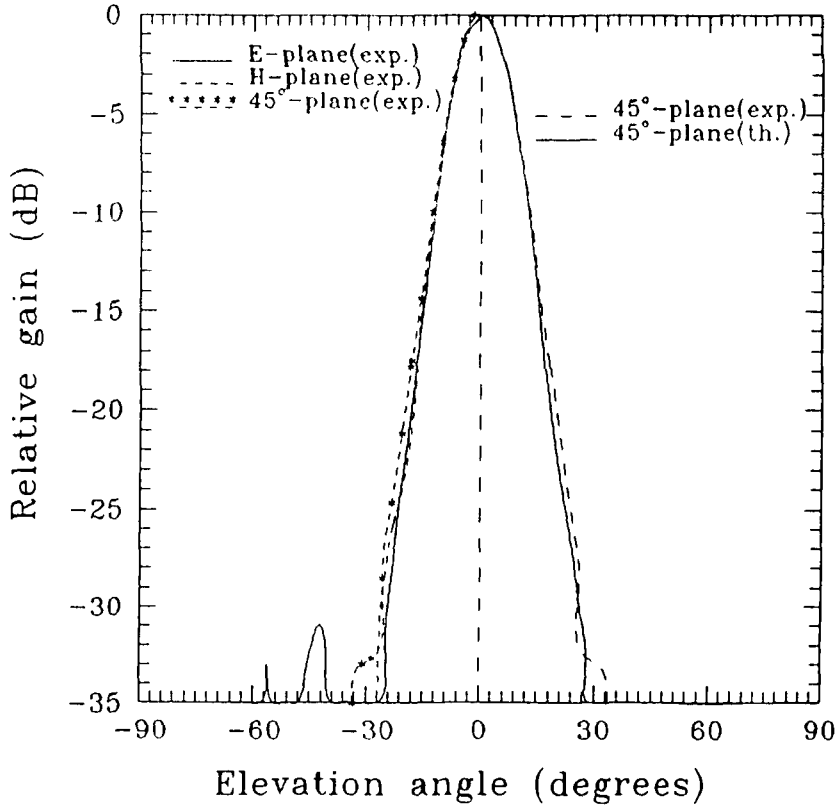

Fig.5 The measured at 370GHz E/H and 45°-plane patterns vs. the full-wave patterns of the 23-dB quasi-integrated horn.

	$0.965f_o$	f_o	$1.035f_o$
Gain	24.7dB	25.5dB	26.2dB
Aperture efficiency	36%	40%	44%
10dB Beamwidth	$21.6 \pm 0.8°$	$19.2° \pm 0.7°$	$17.5° \pm 0.5°$
Sidelobe-level (E-plane)	−28.7dB	−30.8dB	−30.8dB
Cross-pol.(45°)	−22.6dB	−24dB	−24.7dB
Beam-efficiency (to -10dB)	84.5%	85%	85%
Gaussian Coupling	97.1%	97.5%	97.4%
Gaussian Coupling rolloff	96.5%	97.5%	97.1%

Table 5: The main radiation characteristics of the 25dB quasi-integrated horn antenna (see text).

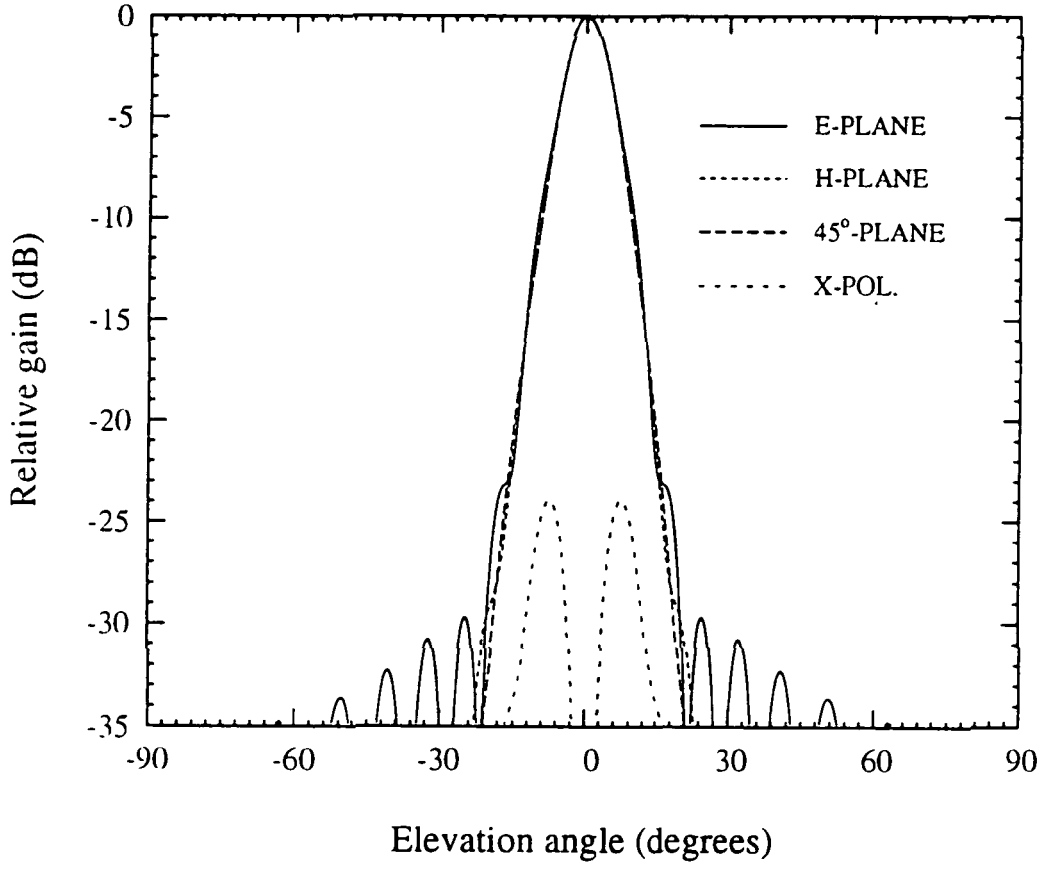

Figure 6: The calculated from the full-wave analysis patterns of the 25-dB quasi-integrated horn.

References

[1] G.M Rebeiz, D.P. Kasilingam, P.A. Stimson, Y. Guo and D.B. Rutledge, "Monolithic millimeter-wave two-dimensional horn imaging arrays," *IEEE Trans. Antennas Propagat.*, vol. AP-28, pp. 1473-1482, Sept 1990.

[2] G.V. Eleftheriades, W.Y. Ali-Ahmad, L.P.B. Katehi, and G.M. Rebeiz, "Millimeter-wave integrated-horn antennas Part I-Theory, and Part II-Experiment," *IEEE Trans. Antennas Propagat.*, vol. AP-39, pp. 1575-1586, Nov. 1991.

[3] G.V. Eleftheriades, W.Y. Ali-Ahmad, and G.M. Rebeiz, "A 20-dB Quasi-integrated horn antenna," *IEEE Microwave and Guided Wave Letters,* vol. 2,pp. 73-75, Feb. 1992.

[4] W.Y. Ali-Ahmad and G.M. Rebeiz, "92GHz dual-polarized integrated horn antennas," *IEEE Trans. Antennas Propagat.,* vol. AP-39, pp. 820-825, June 1991.

[5] W.Y. Ali-Ahmad, Gabriel M. Rebeiz, Hermant Dave, and Gordon Chin "802 GHz Integrated horn antennas imaging array," *International Journal of Infrared and Millimeter Waves,* vol. 12, No. 5.1991.

[6] C.C Ling and G.M Rebeiz, "94GHz Integrated monopulse antenna," IEEE AP-S International Symposium , Ontario, Canada, June 1991.

[7] P.F. Goldsmith, "Quasi-optical techniques at millimeter and submillimeter wavelengths," in *Infrared and Millimeter Waves,* vol. 6, New York : Academic, 1982, pp. 277-243.

[8] E. N. Grossman, "The coupling of submillimeter corner-cube antennas to Gaussian beams," *Infrared Phys.,* vol. 29, pp. 875-885, 1989.

[9] P.D. Potter, "A new horn antenna with suppressed sidelobes and equal beamwidths," *Microwave J.,* vol. VI, pp. 71-78, June 1963.

[10] S.B. Cohn, "Flare-angle changes in a horn as a means of pattern control," *Microwave Journal.,* vol. 13, pp. 41-46, Oct. 1970.

[11] G.V. Eleftheriades, and G.M. Rebeiz, "High-gain step-profiled integrated diagonal horn-antennas," To appear in *IEEE Trans. Microwave Theory Tech.,* mini special issue on Space Terahertz Technology, May 1992.

[12] C. E. Profera, "Complex radiation patterns of dual mode pyramidal horns," *IEEE Trans. Antennas Propagat.,* vol. AP-25, pp. 436-438, May 1977.

[13] L. Solymar, "Spurious mode generation in nonuniform waveguide," *IRE Trans. Microwave Theory Tech.,* vol. MTT-7, pp. 379-383, 1959.